

ANALYTIC LIGHT-CURVES OF GAMMA-RAY BURST AFTERGLOWS:
HOMOGENEOUS VERSUS WIND EXTERNAL MEDIA

A. PANAITESCU

Dept of Astrophysical Sciences, Princeton University, Princeton, NJ 08544

and

P. KUMAR

School of Natural Sciences, Institute for Advanced Study, Princeton, NJ 08540

ABSTRACT

Assuming an adiabatic evolution of a Gamma-Ray Burst (GRB) remnant interacting with an external medium, we calculate the injection, cooling, and absorption break frequencies, and the afterglow flux for plausible orderings of the break and observing frequencies. The analytical calculations are restricted to a relativistic remnant and, in the case of collimated ejecta, to the phase where there is an insignificant lateral expansion. Results are given for both a homogeneous external medium and for a wind ejected by the GRB progenitor.

We compare the afterglow emission at different observing frequencies, for each type of external medium. It is found that observations at sub-millimeter frequencies during the first day provide the best way of discriminating between the two models. By taking into account the effect of inverse Compton (IC) scatterings on the electron cooling, a new possible time-dependence of the cooling break is identified. The signature of the up-scattering losses could be seen in the optical synchrotron emission from a GRB remnant interacting with a pre-ejected wind, as a temporary mild flattening of the afterglow decay. The up-scattered radiation itself should be detected in the soft X-ray emission from GRB remnants running into denser external media, starting few hours after the main event.

Subject headings: gamma-rays: bursts - methods: analytical - radiation mechanisms: non-thermal

1. INTRODUCTION

One of the most important issues regarding Gamma-Ray Bursts (GRBs) is the nature of the object that releases the relativistic ejecta generating the high energy emission of the main event and the lower frequency emission during the ensuing afterglow. Some insight about the GRB progenitor can be obtained from the properties of the circum-burst medium, which can be inferred from the features of the afterglow emission. If the ejecta is expelled during the merging of two compact objects (Mészáros & Rees 1997b), it is expected that the medium surrounding the GRB source is homogeneous. However, if a collapsing massive star (Woosley 1993, Paczyński 1998) is the origin of the relativistic fireball, the circum-burst medium is the wind ejected by the star prior to its collapse, whose density decreases outwards. The two models differ in the dependence on radius of the particle density of the circum-burst medium which the GRB remnant interacts with, and in the value of this density at the deceleration length-scale. The former modifies the rate of decline of the afterglow, while the latter determines the overall afterglow brightness. Therefore it is possible to correlate afterglow emission features to a specific type of external medium.

Significant work in this direction has been done by many researchers. The two afterglows that exhibited breaks consistent with the effects arising from strong collimation of ejecta – GRB 990123 (Kulkarni et al. 1999a) and GRB 990510 (Stanek et al. 1999, Harrison et al. 1999) – indicate that the external gas was homogeneous (recent work by Kumar & Panaitescu 2000 shows that jets interacting with winds cannot produce sharp breaks in the afterglow light-curve). The optical emission of three afterglows had a steeper than usual decline. GRB 970228 decayed as $T^{-1.7}$ after the subtraction of an underlying supernova emission (Reichert 1999, Galama et al. 2000). The

light-curve of GRB 980326 fell off as $T^{-2.1}$ (Groot et al. 1998) and an emission in excess of the early time extrapolation was detected ~ 20 days after the main event, indicating a supernova contribution (Bloom et al. 1999). A T^{-2} decay was observed for the afterglow of GRB 980519 (Halpern et al. 1999). Such steep declines can be produced either by a fireball interacting with a pre-ejected wind (Chevalier & Li 1999) and an electron index around 3, or by a narrow jet expanding laterally in a homogeneous external medium and an electron index slightly larger than 2. Chevalier & Li (1999) found that the radio emission of the afterglow of GRB 980519 is consistent with an external wind; however Frail et al. (2000) point out that the interstellar scintillation present in the radio data does not allow ruling out the jet model. Nevertheless, the existence of supernovae associated with GRB 970228 and GRB 980326 points toward a massive star as the origin of these bursts, implying a pre-ejected wind as the external medium. From the analysis of the optical radio emission of the afterglow of GRB 970508, Chevalier & Li (2000) conclude that the surrounding medium was a wind. Frail, Waxman & Kulkarni (2000) argue that the same radio afterglow can be explained by a homogeneous external medium.

In this work we investigate the differences between the light-curves of afterglows arising for each type of external medium, with the aim of finding ways for distinguishing between the two models. This study is done within the usual framework of a relativistic remnant interacting with a cold external gas. As the fireball is decelerated, a shock front sweeps up the external gas, accelerating relativistic electrons and generating a magnetic field in the shocked gas. We ignore the emission from electrons accelerated by the reverse shock which propagates through the ejecta at very early times. At optical wavelengths this emission is short lived, lasting up to few tens of seconds after the main event (Sari & Piran 1999), but it could be important

for the radio emission until few days (Kulkarni et al. 1999b).

Analytical afterglow light-curves for spherical remnants interacting with homogeneous external media have been previously published by Sari, Piran & Narayan (1998). Features of afterglows from spherical fireballs, such as peak flux, break frequencies, and time evolution of fluxes at a fixed frequency, have been studied by Mészáros & Rees (1997a), Waxman (1997b), Wijers & Galama (1999), and Dai & Lu (2000) for homogeneous media, and by Chevalier & Li (2000) for pre-ejected winds. In this work we present and compare analytical and numerical light-curves at various observing frequencies, covering all cases of interest, for both types of external media, taking into account the differential arrival-time delay and Doppler boosting due to the spherical shape of the source. We take into account first order IC scattering, calculate its effect on the electron cooling and on the afterglow synchrotron emission, and study briefly the high-energy emission resulting from the up-scattering of synchrotron photons. The possible importance of IC scatterings for the early afterglow emission was pointed out by Waxman (1997a) and Wei & Lu (1998).

2. SIMPLE DYNAMICS OF RELATIVISTIC REMNANTS

For the calculation of the afterglow emission it is necessary to know how the remnant Lorentz factor Γ evolves with observer time T , as all other quantities that appear in the expression of the spectral flux are functions of Γ and of the remnant radius r and external medium density $n(r)$. We shall assume that the remnant is adiabatic, i.e. the energy carried away by the emitted photons is a negligible fraction of the total energy of the remnant. This assumption is correct if the energy density of the electrons accelerated at the shock front is a fraction $\varepsilon_e \ll 1$ of the total energy density in post-shock fluid or if most of the electrons are adiabatic, i.e. their radiative cooling timescale exceeds that of the adiabatic losses due to the remnant expansion.

Assuming that the internal energy of the ejecta is negligible compared to its rest-mass energy and that the ratio internal-to-rest mass energy in the energized external medium is $\Gamma - 1$ (i.e. its “temperature” tracks that of the freshly shocked gas), conservation of energy leads to

$$m(r)\Gamma^2 + M_{fb}\Gamma - [m(r) + M_{fb}\Gamma_0] = 0 \quad (1)$$

where M_{fb} and Γ_0 are the initial mass and Lorentz factor of the fireball (whose energy is $E = M_{fb}\Gamma_0$) and

$$m(r) = \frac{4\pi}{3-s} m_p n(r) r^3 \quad (2)$$

is the mass of swept-up material (m_p being the proton’s mass). The external medium particle density is

$$n(r) = Ar^{-s}, \quad (3)$$

with $s = 0$ for a homogeneous medium and $s = 2$ for a wind ejected by the GRB progenitor at a constant speed.

Equation (2) is valid if the remnant is spherical, but can also be used for collimated ejecta when the lateral spreading (Rhoads 1999) is insignificant if the quantity E above is defined as the energy the fireball would have if it were spherical. Throughout this work we shall assume that the remnant is a jet with an initial half-angle larger than $\gtrsim 20^\circ$, in which case the sideways expansion is negligible during the relativistic phase.

The following analytical calculations of the afterglow emission can be extended to sideways expanding jets and non-relativistic remnants by first determining $\Gamma(r)$. The set of coupled differential equations describing the evolution of the jet Lorentz factor and its opening can be solved analytically for $s = 0$ (Rhoads 1999). The lack of a good approximation for the jet dynamics in the case of pre-ejected winds is the main motivation for restricting the following analytical calculations to spherical or wide-angle remnants.

The solution of equation (1) is

$$\Gamma(r) = \frac{1}{2} \left[\sqrt{4x^{3-s} + 1 + (2x^{3-s}/\Gamma_0)^2} - 1 \right] x^{s-3} \Gamma_0, \quad (4)$$

where x is the radial coordinate r scaled to

$$r_0 = \left(\frac{3-s}{4\pi} \frac{E}{m_p c^2 A \Gamma_0^2} \right)^{1/(3-s)}, \quad (5)$$

the deceleration length-scale, at which $m(r_0) = E/(c^2 \Gamma_0^2) = M_{fb}/\Gamma_0$. The result given in equation (4) is also valid in the non-relativistic regime. For $x \ll 1$ $\Gamma \lesssim \Gamma_0$, while for $1 \ll x \ll x_{nr}$ we find $\Gamma = x^{-(3-s)/2} \Gamma_0$. Here $x_{nr} = (\Gamma_0^2/3)^{1/(3-s)}$ marks the end of the relativistic regime: $\Gamma(x_{nr}) = 2$. For the ease of analytical calculations we shall assume that the power-law behavior of Γ lasts from $x = 1$ to $x = x_{nr}$.

The Lorentz factor given in equation (4) represents a “dynamical” average of the Lorentz factors at which different regions of the shocked remnant move (the Blandford – McKee solution). The Lorentz factor of the shock front that propagates into the external gas $\Gamma_{sh} = \sqrt{2}\Gamma$, with Γ given by equation (4), matches that given in equation (69) of Blandford & McKee (1976) for the power-law regime $1 \ll x \ll x_{nr}$ if E is multiplied by $(17-4s)/(12-4s)$. This correction factor ($17/8$ for $s = 0$ and $9/4$ for $s = 2$) will be used in the following results.

The constant A in equation (3) is the number density n_* of the external homogeneous medium for $s = 0$, while for $s = 2$

$$A = \frac{1}{4\pi} \frac{\dot{M}}{m_p v} = 3.0 \times 10^{35} A_* \text{ cm}^{-1}, \quad (6)$$

where \dot{M} is the mass loss rate of the massive star that ejected the wind at constant speed v , and A was scaled to

$$A_* = \frac{\dot{M}/10^{-5} M_\odot \text{ yr}^{-1}}{v/10^3 \text{ km s}^{-1}}, \quad (7)$$

as in Chevalier & Li (2000) for a Wolf-Rayet star. For further calculations it is convenient to use equation (3) in the form $n(r) = n_0(r/r_0)^{-s}$ where $n_0 = n_*$ for $s = 0$, while for $s = 2$

$$n_0 = 1.9 \times 10^4 E_{53}^{-2} \Gamma_{0,2}^4 A_*^3 \text{ cm}^{-3} \quad (8)$$

is the wind particle density at the deceleration radius (eq. [5]):

$$(s = 2) \quad r_0 = 4.0 \times 10^{15} E_{53} \Gamma_{0,2}^{-2} A_*^{-1} \text{ cm}. \quad (9)$$

The usual notation $C_n = 10^{-n} C$ is used throughout this work.

Note that, for the reference values used here, the deceleration radius in the wind model is 1.5 orders of magnitude lower than that for a homogeneous external medium:

$$(s = 0) \quad r_0 = 1.3 \times 10^{17} E_{53}^{1/3} \Gamma_{0,2}^{-2/3} n_{*,0}^{-1/3} \text{ cm}, \quad (10)$$

and even smaller for higher initial fireball Lorentz factors or slower winds (i.e. a larger parameter A_*). If GRBs are due to internal shocks occurring in unstable relativistic fireballs (Rees & Mészáros 1994, Paczyński & Xu 1994, Piran 1999), then the external shock resulting from the interaction of the fireball with the pre-ejected (non-relativistic) wind may occur before the internal shocks are over. In this case successive internal collisions occur when faster parts of the ejecta catch up with the decelerating leading edge of the fireball, a scenario suggested within the $s = 0$ model by Fenimore & Ramirez-Ruiz (2000), but which is more likely to happen if the external medium is the gas ejected by a massive star. The GRB itself would then exhibit the erratic variability characteristic of internal shocks until a time of the order

$$\frac{r_0}{c\Gamma_0^2} \simeq 10 E_{53}\Gamma_{0,2}^{-4}A_*^{-1} s, \quad (11)$$

(which has a strong dependence on Γ_0), after which there may be significant emission from internal shocks on the outermost part of the fireball and from the external shock that plows through the external gas. The former mechanism generates pulses of increasing duration as the fireball expands, while the latter leads to a continuous emission.

The time T when the observer receives a photon emitted along the line of sight toward the fireball center can be calculated by integrating

$$dT = (1 - \beta)dt = \frac{1}{2} \frac{dt}{\Gamma^2}, \quad (12)$$

where β is the shocked fluid speed and $t = r/c$ is the time measured in the laboratory frame. Approximating the solution given in equation (4) with $\Gamma = \Gamma_0$ for $x < 1$ and $\Gamma = x^{-(3-s)/2}\Gamma_0$ for $1 < x < x_{nr}$, one obtains

$$T = T_0(x^{4-s} + 3 - s), \quad T_0 \equiv \frac{1}{2(4-s)} \frac{r_0}{c\Gamma_0^2}. \quad (13)$$

Note that T given in equation (13) is the earliest time a photon emitted by the remnant at time t can reach the observer. Photons emitted by the fluid moving at an angle $\theta = 1/\Gamma$ off the center-observe axis arrive at $T = t(1 - \cos\theta) = t/2\Gamma^2$, which is a factor $4 - s$ larger than the time corresponding to $\theta = 0$: $T = t/2(4 - s)\Gamma^2$.

From equation (13) $r(T)$ can be found and then substituted in the expressions for $\Gamma(r)$ and $n(r)$ to obtain these quantities as a function of the observer time. For the power-law phase the results are

$$(s = 0) \quad \Gamma(T) = 6.3 E_{53}^{1/8} n_{*,0}^{-1/8} T_d^{-3/8}, \quad (14)$$

$$(s = 0) \quad r(T) = 8.2 \times 10^{17} E_{53}^{1/4} n_{*,0}^{-1/4} T_d^{1/4} \text{ cm}, \quad (15)$$

$n = n_*$ (constant) for a homogeneous external medium and

$$(s = 2) \quad \Gamma(T) = 7.9 E_{53}^{1/4} A_*^{-1/4} T_d^{-1/4}, \quad (16)$$

$$(s = 2) \quad r(T) = 6.4 \times 10^{17} E_{53}^{1/2} A_*^{-1/2} T_d^{1/2} \text{ cm}, \quad (17)$$

$$(s = 2) \quad n(T) = 0.73 E_{53}^{-1} A_*^2 T_d^{-1} \text{ cm}^{-3}, \quad (18)$$

for an external wind, T_d being the observer time measured in days. Note that, at least for the scaling values chosen here, Γ , r , and n have about the same values at $T = 1$ day in both models. Also note that the above quantities (and thus the afterglow emission) are independent of the fireball initial Lorentz factor Γ_0 .

3. BREAK FREQUENCIES

Within the synchrotron emission model there are three expected breaks in the afterglow spectrum: (i) an injection break, at the synchrotron frequency ν_i at which the bulk of the electrons injected by the shock front radiate, (ii) a cooling break, at the synchrotron frequency ν_c of electrons whose radiative cooling time equals the expansion timescale, and (iii) an absorption break, at ν_a below which the synchrotron photons are absorbed by electrons in free-free transitions in a magnetic field (synchrotron self-absorption).

The break frequencies can be calculated if the distribution of the injected electrons and the strength of the magnetic field are known. The distribution of the injected electrons is assumed to be $\mathcal{N}_i(\gamma) \propto \gamma^{-p}$ starting from a minimum random Lorentz factor given by

$$\gamma_i = \frac{m_p}{m_e} \varepsilon_e (\Gamma - 1), \quad (19)$$

where m_e is the electron mass. The energy carried by this electron distribution is a fraction $\frac{p-1}{p-2} \varepsilon_e$ of the total internal energy. The post-shock magnetic field strength in the co-moving frame is given by

$$\frac{B^2}{8\pi} = \varepsilon_B m_p c^2 n'_e (\Gamma - 1) = 4\varepsilon_B m_p c^2 n(r) (\Gamma - 1) \left(\Gamma + \frac{3}{4} \right), \quad (20)$$

where ε_B is the fractional energy carried by the magnetic field and n'_e is the co-moving frame electron density behind the shock front. Equations (19) and (20) are based on that the internal to rest-mass energy density ratio in the shocked fluid is $\Gamma - 1$; the derivation of the latter equation also used that the co-moving particle density is $4\Gamma + 3$ times larger than that ahead of the shock.

3.1. Injection Break

Using the relativistic Doppler factor 2Γ corresponding to the motion of the source toward the observer (i.e. $\theta = 0$), the synchrotron emission from a power-law distribution of electrons peaks at the observer frame frequency

$$\nu_i = \frac{3x_p}{2\pi} \frac{e}{m_e c} \gamma_i^2 B \Gamma = 8.4 \times 10^6 x_p \gamma_i^2 B \Gamma \text{ Hz}, \quad (21)$$

where the factor x_p is calculated in Wijers & Galama (1999) for various values of the electron index p . We shall use $x_p = 0.52$, which is strictly correct only for $p = 2.5$. With the aid of equations (14), (16), (18), (19), and (20) one obtains:

$$(s = 0) \quad \nu_i = 0.92 \times 10^{13} E_{53}^{1/2} \varepsilon_{e,-1}^2 \varepsilon_{B,-2}^{1/2} T_d^{-3/2} \text{ Hz}, \quad (22)$$

$$(s = 2) \quad \nu_i = 1.9 \times 10^{13} E_{53}^{1/2} \varepsilon_{e,-1}^2 \varepsilon_{B,-2}^{1/2} T_d^{-3/2} \text{ Hz}. \quad (23)$$

Note that ν_i has the same scalings with the model parameters for $s = 0$ and $s = 2$. The ratio of the two frequencies is $\sqrt{\frac{17}{72}}$.

3.2. Cooling Break

The relativistic electrons cool radiatively through synchrotron emission and IC scatterings of the synchrotron photons on a co-moving frame timescale

$$t'_{rad}(\gamma) = \frac{t'_{sy}(\gamma)}{Y+1} = \frac{6\pi}{Y+1} \frac{m_e c}{\sigma_e} \frac{1}{\gamma B^2}, \quad (24)$$

where $t'_{sy}(\gamma)$ is the co-moving frame synchrotron cooling timescale of electrons of Lorentz factor γ , Y is the Compton parameter, and σ_e the cross-section for electron scatterings¹. Using equation (20), the Lorentz factor of the electrons that cool radiatively on a timescale equal to the remnant age

$$t' = \frac{1}{c} \int \frac{dr}{\Gamma} = \frac{2}{5-s} \frac{r}{c\Gamma} \quad (25)$$

can be written as

$$\gamma_c = \frac{3\pi(5-s)}{Y+1} \frac{m_e c^2}{\sigma_e} \frac{\Gamma}{B^2 r} = \frac{77(5-s)}{(Y+1)\varepsilon_B n\Gamma r_{18}}, \quad (26)$$

with n in cm^{-3} .

The observer-frame frequency ν_c of the cooling break is

$$(s=0) \quad \nu_c = 3.7 \times 10^{14} E_{53}^{-1/2} n_{*,0}^{-1} (Y+1)^{-2} \varepsilon_{B,-2}^{-3/2} T_d^{-1/2} \text{ Hz}, \quad (27)$$

$$(s=2) \quad \nu_c = 3.5 \times 10^{14} E_{53}^{1/2} A_*^{-2} (Y+1)^{-2} \varepsilon_{B,-2}^{-3/2} T_d^{1/2} \text{ Hz}. \quad (28)$$

Hereafter we shall use the terminology ‘‘radiative electrons’’ for the case where the γ_i -electrons cool mostly through emission of radiation (i.e. $t'_{rad}(\gamma_i) < t'$ and $\gamma_c < \gamma_i$), and we shall refer to ‘‘adiabatic electrons’’ if the γ_i -electrons cool mostly adiabatically (i.e. $t'_{rad}(\gamma_i) > t'$ and $\gamma_i < \gamma_c$).

3.2.1. Compton Parameter and Electron Distribution

For the calculation of the Compton parameter Y , we take into account only one up-scattering of the synchrotron photons. Multiple IC scatterings of the same photon have an important effect on the electron cooling only if the Y parameter for single scatterings is above unity. As shown in §3.2.2 and §3.2.3 this occurs if 1) $\varepsilon_B \lesssim 10^{-2} \varepsilon_{e,-1}$ and if 2) $T < T_y$, where T_y is the time when Y falls below unity.

Using equations (19) and (20), it can be shown that IC scatterings of order higher than two are suppressed by the Klein-Nishina effect. For adiabatic electrons, a second IC scattering occurs in the Thomson regime if 3a) $T \gtrsim 1 E_{53}^{1/3} n_{*,0}^{-1/9} \varepsilon_{e,-1}^{20/9} \varepsilon_{B,-4}^{2/9}$ d for $s=0$, and if 3b) $T \gtrsim 1 E_{53}^{1/2} A_*^{-1/4} \varepsilon_{e,-1}^{5/2} \varepsilon_{B,-4}^{1/4}$ d for $s=2$. If a second IC scattering is ignored in these cases then a higher energy component peaking around 1 GeV is left out, otherwise the synchrotron and first IC emissions remain unaltered if the electrons are adiabatic.

The effect of second order up-scatterings is more important when electrons are radiative, i.e. for 4) $T < T_r$ with T_r calculated in §3.2.2, as in this case it reduces the intensity of the synchrotron and first stage IC components. With the aid of equations (19) and (20) it can be shown that for $s=0$ a second up-scattering occurs in the Thomson regime and at $T > 10^{-2}$ d if 5a) $n \gtrsim 25 E_{53}^{-7/11} \varepsilon_{e,-1}^{-10/11} \varepsilon_{B,-3}^{-2/11} \text{ cm}^{-3}$, while for $s=2$

the second IC emission is not suppressed by the Klein-Nishina effect if 5b) $T \gtrsim 0.05 E_{53}^{-1/3} A_*^{11/6} \varepsilon_{e,-1}^{5/6} \varepsilon_{B,-3}^{2/3}$ d.

Concluding, second stage up-scatterings can be ignored if the set of conditions 1), 2), 3) or 1), 4), 5) are not simultaneously satisfied. For a single up-scattering, the Compton parameter is

$$Y = \frac{4}{3} \int_{\mathcal{N}_e} \gamma^2 d\tau_e = \frac{4}{3} \tau_e \int_{\mathcal{N}_e} \gamma^2 \mathcal{N}_e(\gamma) d\gamma, \quad (29)$$

where $\mathcal{N}_e(\gamma)$ is the normalized electron distribution and τ_e is the optical thickness to electron scattering, given by

$$\tau_e = \frac{1}{4\pi} \frac{\sigma_e m(r)}{m_p r^2} = \frac{1}{3-s} \sigma_e n r. \quad (30)$$

If the injected γ_i -electrons cool faster than the timescale of their injection, then γ_c given by equation (26) is the typical electron Lorentz factor in the remnant, and the electron distribution in the shocked fluid can be approximated by

$$\mathcal{N}_e^{(r)} \propto \begin{cases} \gamma^{-2} & \gamma_c < \gamma < \gamma_i \\ \gamma^{-(p+1)} & \gamma_i < \gamma \end{cases}, \quad (31)$$

with $p > 2$. In the opposite case most electrons have a random Lorentz factor γ_i , and the electron distribution is

$$\mathcal{N}_e^{(a)} \propto \begin{cases} \gamma^{-p} & \gamma_i < \gamma < \gamma_c \\ \gamma^{-(p+1)} & \gamma_c < \gamma \end{cases}. \quad (32)$$

3.2.2. Radiative Electrons

For $\gamma_c \ll \gamma_i$ equations (29) and (31) lead to

$$Y_r = \frac{4}{3} \gamma_i \gamma_c \tau_e. \quad (33)$$

Substituting γ_c with the aid of equation (26), one obtains

$$Y_r(Y_r + 1) = \frac{5-s}{8(3-s)} \frac{n'_e m_e c^2 \gamma_i}{B^2/8\pi} = \frac{5-s}{8(3-s)} \frac{\varepsilon_e}{\varepsilon_B}, \quad (34)$$

where we used equations (19) and (20). Therefore the Compton parameter during the electron radiative phase is

$$Y_r = \frac{1}{2} \left(\sqrt{\frac{5-s}{2(3-s)} \frac{\varepsilon_e}{\varepsilon_B} + 1} - 1 \right). \quad (35)$$

Hence the electron cooling is dominated by IC scatterings (i.e. $Y_r > 1$) for $\varepsilon_B < \tilde{\varepsilon}_B$, where

$$\tilde{\varepsilon}_B = \frac{5-s}{16(3-s)} \varepsilon_e. \quad (36)$$

Note that Y_r is time-independent. Therefore the ν_c given by equations (27) and (28) decreases with time for $s=0$ and increases in the $s=2$ model. Thus, for observations made at a fixed frequency, the electrons emitting at that frequency change their cooling regime from adiabatic to radiative in the case of a homogeneous external gas, and from radiative to adiabatic for an external wind (Chevalier & Li 2000).

¹ The up-scattering of the ν_i synchrotron photons on the γ_c - and γ_i -electrons occurs in the Thomson regime for $T > 10^{-3}$ day, i.e. the scattering cross-section in equation (24) is not reduced by the Klein-Nishina effect

With the aid of equations (19), (20), and (24), it can be shown that the electrons are radiative if

$$nr\Gamma^2 > \frac{3(5-s)}{32(Y_r+1)} \frac{(m_e/m_p)^2}{\sigma_e \varepsilon_e \varepsilon_B} = \frac{4.2 \times 10^{16}}{\varepsilon_e \varepsilon_B} \frac{5-s}{Y_r+1} \text{ cm}^{-2}, \quad (37)$$

which, with the further use of equations (14) – (18), leads to the conclusion that the electrons are radiative until the observer time T_r given by

$$(s=0) \quad T_r = 0.025 E_{53} n_{*,0} (Y_r+1)^2 \varepsilon_{e,-1}^2 \varepsilon_{B,-2}^2 \text{ day}, \quad (38)$$

$$(s=2) \quad T_r = 0.23 A_* (Y_r+1) \varepsilon_{e,-1} \varepsilon_{B,-2} \text{ day}. \quad (39)$$

3.2.3. Adiabatic Electrons

For $\gamma_i \ll \gamma_c$ equations (29) and (32) give the Compton parameter

$$Y_a = \frac{4}{3} \tau_e \times \begin{cases} \gamma_i^{p-1} \gamma_c^{3-p} & 2 < p < 3 \\ \gamma_i^2 & 3 < p \end{cases}. \quad (40)$$

Case 1: $2 < p < 3$. By substituting equations (19) and (26) in equation (40), one obtains

$$Y_a (Y_a + 1)^{3-p} = \mathcal{F}_p(T) \equiv c_s(p) \varepsilon_e^{p-1} \varepsilon_B^{-p-3} (n\Gamma^2 r_{18})^{p-2}, \quad (41)$$

where $\log c_s(p) = (3-p) \log(5-s) - \log(3-s) + 1.4p - 3.7$. The Compton parameter can be obtained by solving numerically the above equation. For analytical purposes, one can approximate $Y_a = \mathcal{F}_p$ for $\mathcal{F}_p < 1$, in which case the IC losses are less important, and

$$Y_a = \mathcal{F}_p^{\frac{1}{4-p}} \quad \text{for } \mathcal{F}_p > 1. \quad (42)$$

In the latter case the IC scatterings affect the electron cooling.

Note that the quantity $n\Gamma^2 r$ in equation (41) decreases with time. Thus, for $\varepsilon_B < \tilde{\varepsilon}_B$, the Compton parameter Y_a is above unity until a time T_y which can be determined by substituting equations (14) – (18) in (42):

$$(s=0) \quad T_y = 10^{\frac{8-3p}{p-2}} E_{53} n_{*,0} \varepsilon_{e,-1}^{\frac{2p-1}{p-2}} \varepsilon_{B,-3}^{-\frac{2(3-p)}{p-2}} \text{ day}, \quad (43)$$

$$(s=2) \quad T_y = 10^{\frac{4.9-1.6p}{p-2}} A_* \varepsilon_{e,-1}^{\frac{p-1}{p-2}} \varepsilon_{B,-3}^{-\frac{3-p}{p-2}} \text{ day}. \quad (44)$$

Thus, for $\varepsilon_B < \tilde{\varepsilon}_B$ and $T_r < T < T_y$, the Compton parameter determines the evolution of the cooling break frequency (eqs. [27] and [28]):

$$\nu_c \stackrel{(s=0)}{=} 10^{15 + \frac{2.5p-5.5}{4-p}} \left[E_{53}^{-\frac{p}{2}} n_{*,0}^{-2} \varepsilon_{e,-1}^{-2(p-1)} \varepsilon_{B,-3}^{-\frac{p}{2}} T_d^{\frac{3p-8}{2}} \right]^{\frac{1}{4-p}} \text{ Hz}, \quad (45)$$

$$\nu_c \stackrel{(s=2)}{=} 10^{15 + \frac{2.5p-5.5}{4-p}} E_{53}^{\frac{1}{2}} \left[A_*^{-4} \varepsilon_{e,-1}^{-2(p-1)} \varepsilon_{B,-3}^{-\frac{p}{2}} T_d^{\frac{3p-4}{2}} \right]^{\frac{1}{4-p}} \text{ Hz}. \quad (46)$$

Note that for a homogeneous medium ($s=0$) and $8/3 < p < 3$, the cooling break frequency increases with time, unlike the decreasing behavior it has for $T < T_r$.

Case 2: $p > 3$. This case is treated here for completeness, as there are no afterglows for which such a steep electron index has been found. Equations (19), (30), and (40) lead to

$$Y_a = \frac{3}{3-s} \varepsilon_e^2 n\Gamma^2 r_{18}. \quad (47)$$

For $\varepsilon_B < \tilde{\varepsilon}_B$ the Compton parameter is above unity until

$$(s=0) \quad T_y = 0.11 E_{53} n_{*,0} \varepsilon_{e,-1}^4 \text{ day}, \quad (48)$$

$$(s=2) \quad T_y = 0.87 A_* \varepsilon_{e,-1}^2 \text{ day}. \quad (49)$$

For $\varepsilon_B < \tilde{\varepsilon}_B$ and $T_r < T < T_y$, the evolution of the cooling break frequency is

$$(s=0) \quad \nu_c = 1.1 \times 10^{17} E_{53}^{-3/2} n_{*,0}^{-2} \varepsilon_{e,-1}^{-4} \varepsilon_{B,-3}^{-3/2} T_d^{1/2} \text{ Hz}, \quad (50)$$

$$(s=2) \quad \nu_c = 1.5 \times 10^{16} E_{53}^{1/2} A_*^{-4} \varepsilon_{e,-1}^{-4} \varepsilon_{B,-3}^{-3/2} T_d^{5/2} \text{ Hz}. \quad (51)$$

Note that in this regime ν_c increases with time in both models.

3.3. Absorption Break

The synchrotron self-absorption frequency ν_a can be calculated with the aid of equation (6.50) from Rybicki & Lightman (1979). With the notations $\gamma_p = \min(\gamma_i, \gamma_c)$, $\nu_p = \min(\nu_i, \nu_c)$, and $\nu_0 = \max(\nu_i, \nu_c)$ it can be shown that optical thickness to synchrotron self-absorption can be approximated by

$$\tau_{ab}(\nu) \simeq 5 \frac{e\Sigma}{B\gamma_p^5} \times \begin{cases} (\nu/\nu_p)^{-5/3} & \nu < \nu_p \\ (\nu/\nu_p)^{-(q+4)/2} & \nu_p < \nu < \nu_0 \end{cases}, \quad (52)$$

where $\Sigma = (3-s)^{-1} nr$ is the remnant electron column density, $q = 2$ for radiative electrons ($\gamma_c < \gamma_i$), $q = p$ for adiabatic electrons ($\gamma_i < \gamma_c$).

3.3.1. Radiative Electrons

Equations (20), (26), and (52) give the optical thickness at the cooling break frequency

$$\tau_c = \frac{5}{3-s} \frac{enr}{B\gamma_c^5} = \frac{1.1 \times 10^{-3}}{(3-s)(5-s)^5} (Y_r+1)^5 \varepsilon_B^{9/2} n^{11/2} \Gamma^4 r_{18}^6. \quad (53)$$

For $s=0$ equations (14), (15), and (53) lead to

$$(s=0) \quad \tau_c = 0.11 E_{53}^2 n_{*,0}^{7/2} (Y_r+1)^5 \varepsilon_B^{9/2}. \quad (54)$$

For $\tau_c < 1$ the optical thickness to synchrotron self-absorption is unity at ν_a given by $\nu_a = \nu_c \tau_c^{3/5}$:

$$(s=0) \quad \nu_a = 6.5 \times 10^9 E_{53}^{7/10} n_{*,0}^{11/10} (Y_r+1) \varepsilon_{B,-1}^{6/5} T_d^{-1/2} \text{ Hz}. \quad (55)$$

For $s=2$ equations (16) – (18), and (53) give

$$(s=2) \quad \tau_c = 0.44 E_{53}^{-3/2} A_*^7 (Y_r+1)^5 \varepsilon_B^{9/2} T_d^{-7/2}. \quad (56)$$

For $T > T_a$ we have $\tau_c < 1$ and $\nu_a < \nu_c$:

$$(s=2) \quad \nu_a = 1.4 \times 10^{12} E_{53}^{-2/5} A_*^{11/5} (Y_r+1) \varepsilon_{B,-2}^{6/5} T_{d,-2}^{-8/5} \text{ Hz}. \quad (57)$$

3.3.2. Adiabatic Electrons

The optical thickness to synchrotron self-absorption at the injection break can be found using equations (19), (20), and (52):

$$\tau_i = \frac{5}{3-s} \frac{enr}{B\gamma_i^5} = \frac{2.9 \times 10^{-2}}{3-s} \frac{n^{1/2} r_{18}}{\varepsilon_{e,-1}^5 \varepsilon_B^{1/2} \Gamma^6}. \quad (58)$$

If the external medium is homogeneous

$$(s=0) \quad \tau_i = 1.3 \times 10^{-6} E_{53}^{-1/2} n_{*,0} \varepsilon_{e,-1}^{-5} \varepsilon_{B,-2}^{-1/2} T_d^{5/2}, \quad (59)$$

$$(s=0) \quad \nu_a = 2.6 \times 10^9 E_{53}^{1/5} n_{*,0}^{3/5} \varepsilon_{e,-1}^{-1} \varepsilon_{B,-2}^{1/5} \text{ Hz}, \quad (60)$$

which is time-independent.

For the wind model

$$(s=2) \quad \tau_i = 6.8 \times 10^{-7} E_{53}^{-3/2} A_*^2 \varepsilon_{e,-1}^{-5} \varepsilon_{B,-2}^{-1/2} T_d^{3/2}, \quad (61)$$

$$(s=2) \quad \nu_a = 3.7 \times 10^9 E_{53}^{-2/5} A_*^{6/5} \varepsilon_{e,-1}^{-1} \varepsilon_{B,-2}^{1/5} T_d^{-3/5} \text{ Hz}. \quad (62)$$

Note that, in general, the absorption frequency decreases faster for a remnant interacting with a wind than for one running into a homogeneous external medium.

4. ANALYTICAL LIGHT-CURVES

If the effects arising from the remnant spherical shape (see Appendix) are ignored, than the observed flux peaks at $\nu_p = \min(\nu_i, \nu_c)$, where it has a value

$$F_{\nu_p} \simeq \frac{\sqrt{3}\phi_p}{4\pi D^2} \frac{e^3}{m_e c^2} \Gamma B N_e. \quad (63)$$

Here ϕ_p is a factor calculated by Wijers & Galama (1999), which we shall set $\phi_p = 0.63$, $D = (1+z)^{-1/2} D_l(z)$ with D_l the luminosity distance, and $N_e = m(r)/m_p$ is the number of electrons in the remnant. Equations (19), (20), and (63) give

$$F_{\nu_p} = \frac{57}{3-s} D_{28}^{-2} \varepsilon_B^{1/2} \Gamma^2 n^{3/2} r_{18}^3 \text{ mJy}. \quad (64)$$

The afterglow emission at any given frequency and time can be calculated using the synchrotron spectrum for the electron distributions given in equations (31) and (32) (e.g. Sari et al. 1998):

$$F_\nu = F_{\nu_c} \begin{cases} (\nu/\nu_a)^2 (\nu_a/\nu_c)^{1/3} & \nu < \nu_a & (1) \\ (\nu/\nu_c)^{1/3} & \nu_a < \nu < \nu_c & (2) \\ (\nu/\nu_c)^{-1/2} & \nu_c < \nu < \nu_i & (3) \\ (\nu/\nu_i)^{-p/2} (\nu_c/\nu_i)^{1/2} & \nu_i < \nu & (4) \end{cases} \quad (65)$$

for $T < T_r$, assuming that $\nu_a < \nu_c$, and

$$F_\nu = F_{\nu_i} \begin{cases} (\nu/\nu_a)^2 (\nu_a/\nu_i)^{1/3} & \nu < \nu_a & (5) \\ (\nu/\nu_i)^{1/3} & \nu_a < \nu < \nu_i & (6) \\ (\nu/\nu_i)^{-(p-1)/2} & \nu_i < \nu < \nu_c & (7) \\ (\nu/\nu_c)^{-p/2} (\nu_i/\nu_c)^{(p-1)/2} & \nu_c < \nu & (8) \end{cases} \quad (66)$$

for $T > T_r$, assuming that $\nu_a < \nu_i$.

In Figures 1 and 2 the plane $T - \varepsilon_B$ is divided into several regions which are labeled as in equations (65)–(66), according to the ordering of the observing frequency ν and of the three

break frequencies ν_a , ν_i , and ν_c . The observed fluxes in each case are given in the Appendix, and a set of multi-wavelength light-curves is shown in Figure 3. The results shown in Figures 1–4 have been obtained using equations which are valid in any relativistic regime, such as equations (4), (19), (20), and (63).

4.1. Inverse Compton Emission

The IC emission can be easily calculated by using the above equations for the synchrotron spectrum and Compton parameter. The up-scattered spectrum peaks at $\nu_{ic} \sim \gamma_c^2 \nu_c$ if electrons are radiative and at $\nu_{ic} \sim \gamma_i^2 \nu_i$ if electrons are adiabatic. It can be shown that, for any electron radiative regime, the flux of the up-scattered emission at this frequency is

$$F_{\nu_{ic}}^{(ic)} = \tau_e F_{\nu_p}, \quad (67)$$

where τ_e and F_{ν_p} are given by equations (30) and (64), respectively. For the up-scattering of synchrotron photons above ν_a and assuming that $Y_a < 1$, the resulting IC light-curves have the following behaviors:

$$\left(\begin{array}{l} s=0 \\ T < T_r \end{array} \right) \quad F_\nu^{(ic)} \propto \begin{cases} T^{1/3} & \nu \lesssim \gamma_c^2 \nu_c \\ T^{1/8} & \gamma_c^2 \nu_c \lesssim \nu \lesssim \gamma_i^2 \nu_i \\ T^{-(9p-10)/8} & \gamma_i^2 \nu_i \lesssim \nu \end{cases}, \quad (68)$$

$$\left(\begin{array}{l} s=0 \\ T > T_r \end{array} \right) \quad F_\nu^{(ic)} \propto \begin{cases} T^1 & \nu \lesssim \gamma_i^2 \nu_i \\ T^{-(9p-11)/8} & \gamma_i^2 \nu_i \lesssim \nu \lesssim \gamma_c^2 \nu_c \\ T^{-(9p-10)/8} & \gamma_c^2 \nu_c \lesssim \nu \end{cases}, \quad (69)$$

$$\left(\begin{array}{l} s=2 \\ T < T_r \end{array} \right) \quad F_\nu^{(ic)} \propto \begin{cases} T^{-5/3} & \nu \lesssim \gamma_c^2 \nu_c \\ T^0 & \gamma_c^2 \nu_c \lesssim \nu \lesssim \gamma_i^2 \nu_i \\ T^{-(p-1)} & \gamma_i^2 \nu_i \lesssim \nu \end{cases}, \quad (70)$$

$$\left(\begin{array}{l} s=2 \\ T > T_r \end{array} \right) \quad F_\nu^{(ic)} \propto \begin{cases} T^{-1/3} & \nu \lesssim \gamma_i^2 \nu_i \\ T^{-p} & \gamma_i^2 \nu_i \lesssim \nu \lesssim \gamma_c^2 \nu_c \\ T^{-(p-1)} & \gamma_c^2 \nu_c \lesssim \nu \end{cases}. \quad (71)$$

For external media that are not denser than assumed so far, the IC emission is weaker than synchrotron, even in soft X-rays. As shown in the upper left panel of Figure 3, for $n_* \gtrsim 10 \text{ cm}^{-3}$ and $A_* \gtrsim 1$ the up-scattered radiation can dominate the synchrotron emission at times $T \gtrsim 10^{-1}$ day, diminishing the decay rate of the X-ray emission. This is due to that the flux at the IC peak (eq. [67]) depends strongly on the external medium density: $F_{\nu_{ic}}^{(ic)} \propto n_*^{5/4}$ for $s=0$ and $F_{\nu_{ic}}^{(ic)} \propto A_*^{5/2}$ for $s=2$. The afterglow flattening is strongly dependent on the observing frequency, being absent in the optical and below.

5. CONCLUSIONS

Using the analytical results given in equations (B1)–(C9), the afterglow light-curve can be calculated at any frequency and at observing times up to the onset of the non-relativistic phase. As illustrated in Figure 3, the largest differences between the afterglow emission in the two models for the external medium is seen at low frequencies (lower panels). However, the scintillation due to the local interstellar medium (Goodman 1997), may hamper the use of the radio light-curves to identify the type of external medium and geometry of the ejecta (Frail et al. 2000).

Figure 4 shows that, for various model parameters, the rate of change of the afterglow emission at $\nu \sim 10^{12}$ Hz and at early times (when the jet effects are negligible, provided that

the jet is initially wider than a few degrees) exhibits a strong dependence on the type of external medium. If the external medium is homogeneous the sub-millimeter afterglow should rise slowly at times between ~ 1 hour and ~ 1 day, while for a pre-ejected wind the emission should fall off steeply, followed by a plateau². Therefore observations made at sub-millimeter frequencies with the SCUBA (James Clerk Maxwell Telescope) or with the MAMBO (IRAM Telescope) instruments would be very powerful in determining if the medium which the remnant runs into is homogeneous or follows a r^{-2} law.

We note that if turbulence in the shocked fluid does not lead to a significant mixing, then the inhomogeneous electron distribution will alter the afterglow spectrum below the absorption frequency ν_a as described by Granot, Piran & Sari (2000). The result is that the afterglow emission at $\nu < \nu_a$ rises more slowly than calculated here. For instance, the T^2 rise exhibited by the $\nu = 10^{12}$ Hz light-curves shown in Figure 4 for the wind model at early times becomes a T^1 rise. Nevertheless, the basic difference mentioned above between the temporal behaviors of the sub-millimeter light-curves at $10^{-2} \text{ day} \lesssim T \lesssim 1 \text{ day}$ remains unchanged.

The IC losses alter the evolution of the cooling break ν_c if the electrons injected with minimal energy are adiabatic and if the Compton parameter is above unity (i.e. the magnetic field parameter is weaker than that given in eq. [36]). In the case of a homogeneous external medium, the cooling break frequency decreases as $T^{-1/2}$ if the electrons are radiative. When the electrons become adiabatic, this break evolves as $T^{\frac{3p-8}{8-2p}}$ for $p < 3$ and increases as $T^{1/2}$ for $p > 3$. For an external wind

the change is from $\nu_c \propto T^{1/2}$ to $\nu_c \propto T^{\frac{3p-4}{8-2p}}$ for $p < 3$, and to $\nu_c \propto T^{5/2}$ for $p > 3$. Consequently the power-law decay of the afterglow emission at frequencies above the cooling break flattens by up to 1/2 if the external medium is homogeneous and by up to 1 if the medium is a wind. For an electron index $p < 3$, the flattening is mild and likely to be seen only in the optical emission from a remnant interacting with a pre-ejected wind.

The IC emission itself is generally weaker than the synchrotron emission. Nevertheless, if the external medium is sufficiently dense (i.e. $n_* \gtrsim 10 \text{ cm}^{-3}$ or $A_* \gtrsim \text{few}$), a flattening of the soft X-ray light-curve should be seen few hours after the main event, at fluxes well above the threshold of BeppoSAX (see Figure 3, upper left panel). The flattening of the afterglow emission due to the up-scattered radiation is a chromatic feature, appearing only at high frequencies, and its strength is moderately dependent on the remaining model parameters.

Finally, another possible signature of the interaction with the wind ejected by a Wolf-Rayet star should be found during the GRB emission in the form of smooth pulses of increasing duration. Such pulses are generated in internal shocks when the decelerating outermost shell is hit from behind by shells ejected at later times. This phenomenon is more likely to be seen in the wind model, for which the deceleration radius is smaller than for a homogeneous medium.

AP acknowledges the support received from Princeton University through the Lyman Spitzer, Jr. Fellowship. We thank Bohdan Paczyński for useful discussions.

APPENDIX

The observer time calculated with equation (12) is the time when photons emitted by the shocked gas moving precisely toward the observer arrive at detector. Photons emitted by the fluid moving at a non-zero angle relative to the direction toward the observer are less boosted by the relativistic motion of the source and arrive at the observer later. The effect of the remnant spherical curvature on the afterglow emission can be reduced to a correction factor that must be applied to the light-curve obtained analytically using the remnant parameters at laboratory frame time t related to the observer time T through equation (12). This correction factor is dependent on the observing frequency, as described below.

CORRECTION FACTORS FOR ANALYTICAL LIGHT-CURVES

The flux received by the observer at time T can be calculated by integrating the remnant emission over the equal arrival-time surface (Panaitescu & Mészáros 1998). This surface is defined by $cT = ct - r \cos \theta$, where θ is the azimuthal angle measured relative to the observer's line of sight toward the remnant center. Using the equation for dynamics of relativistic remnants ($\Gamma \propto r^{-(3-s)/2}$), the integral can be written as

$$F_\nu(T) = \frac{A(cT)^{-2}}{2(3-s)D^2} \int_0^{R(T)} \frac{(P'_{\nu'})_e r^{4-s}}{\Gamma^3(x+1)^2} dr, \quad (\text{A1})$$

where $x \equiv (3-s)(r/R)^{4-s}$, and R is the radius for which photons emitted at $\theta = 0$ arrive at T , i.e. the maximal radius on the equal arrival-time surface. In equation (A1) $(P'_{\nu'})_e$ is the co-moving frame power per electron, taking into account the spectrum of the emission. For the synchrotron spectra given in equations (65) and (66), one can write generically $(P'_{\nu'})_e = \sqrt{3}\phi_p(e^3 B/m_e c^2)(\nu'/\nu'_a)^{\alpha_a}(\nu'/\nu'_i)^{\alpha_i}(\nu'/\nu'_c)^{\alpha_c}$, where ν' is the co-moving frame observing frequency. The integral in equation (A1) is determined by the values at of the integrand at $r \lesssim R$.

If the effect of the remnant geometrical curvature on the photon arrival-time were ignored, then the observed flux would be

$$F_\nu^{(0)}(R) = \frac{1}{4\pi D^2} [(P'_{\nu'})_e \Gamma N_e]_{R(T)}, \quad (\text{A2})$$

which can be calculated based on equations (63), (65) and (66). The r -dependent quantities in equation (A1) can be expressed in

²The light-curves presented in the upper left panel of Figure 4 show that this criterion for determining the type of external medium fails only if the particle density of the homogeneous medium exceeds $\sim 10 \text{ cm}^{-3}$. In this case the X-ray emission may help to distinguish between the two models of external medium, as the absence of a flattening of the high energy emission is compatible only with a pre-ejected wind with A_* less than a few.

terms of their values at $r = R$, so that the flux F_ν can be written as $F_\nu^{(0)}$ times a correction factor

$$K = 2(4-s)^{2-(\alpha_a+\alpha_i+\alpha_c)} \int_0^1 u^{f(s)} [1 + (3-s)u^{4-s}]^{\alpha_a+\alpha_i+\alpha_c-2} du, \quad (\text{A3})$$

where $f(s) = 7 - 2.5s - 2\alpha_a(q - 3s) + \alpha_i(2 - 0.5s) - \alpha_c(2 + 0.5s)$, with $q = 1, 2$ for radiative, radiative electrons, respectively. The K factor depends on ν and also on p if $\nu > \nu_i$. Table 1 gives its values for various cases.

HOMOGENEOUS EXTERNAL MEDIUM ($S = 0$)

By substituting the equations for the break frequencies and equation (64) in equations (65) and (66), and taking into account the above correction factors for the remnant curvature, the following fluxes are obtained

$$F_\nu \stackrel{(1)}{=} 0.3 D_{28}^{-2} (Y_r + 1)^{-1} n_{*,0}^{-1} \varepsilon_{B,-1}^{-1} \nu_{9.7}^2 T_{d,-1} \text{ mJy}, \quad (\text{B1})$$

$$F_\nu \stackrel{(2)}{=} 10 D_{28}^{-2} (Y_r + 1)^{2/3} E_{53}^{7/6} n_{*,0}^{5/6} \varepsilon_{B,-2} \nu_{14.6}^{1/3} T_{d,-2}^{1/6} \text{ mJy}, \quad (\text{B2})$$

$$F_\nu \stackrel{(3)}{=} 40 D_{28}^{-2} (Y_r + 1)^{-1} E_{53}^{3/4} \varepsilon_{B,-1}^{-1/4} \nu_{14.6}^{-1/2} T_{d,-2}^{-1/4} \text{ mJy}, \quad (\text{B3})$$

$$F_\nu \stackrel{(4)}{=} 10^{2.1-0.6p} D_{28}^{-2} (Y_r + 1)^{-1} E_{53}^{\frac{p+2}{4}} \varepsilon_{e,-1}^{p-1} \varepsilon_{B,-1}^{\frac{p-2}{4}} \nu_{14.6}^{-\frac{p}{2}} T_d^{-\frac{3p-2}{4}} \text{ mJy}, \quad (\text{B4})$$

$$F_\nu \stackrel{(5)}{=} 30 D_{28}^{-2} E_{53}^{1/2} n_{*,0}^{-1/2} \varepsilon_{e,-1} \nu_{9.7}^2 T_{d,1}^{1/2} \text{ mJy}, \quad (\text{B5})$$

$$F_\nu \stackrel{(6)}{=} 1 D_{28}^{-2} E_{53}^{5/6} n_{*,0}^{1/2} \varepsilon_{e,-1}^{-2/3} \varepsilon_{B,-4}^{1/3} \nu_{14.6}^{1/3} T_{d,-2}^{1/2} \text{ mJy}, \quad (\text{B6})$$

$$F_\nu \stackrel{(7)}{=} 10^{2.1-1.3p} D_{28}^{-2} E_{53}^{\frac{p+3}{4}} n_{*,0}^{1/2} \varepsilon_{e,-1}^{p-1} \varepsilon_{B,-4}^{\frac{p+1}{4}} \nu_{14.6}^{-\frac{p-1}{2}} T_d^{-\frac{3}{4}(p-1)} \text{ mJy}, \quad (\text{B7})$$

$$F_\nu \stackrel{(8)}{=} 10^{2.4-0.8p} D_{28}^{-2} E_{53}^{\frac{p+2}{4}} \varepsilon_{e,-1}^{p-1} \varepsilon_{B,-2}^{\frac{p-2}{4}} \nu_{14.6}^{-\frac{p}{2}} T_d^{-\frac{3p-2}{4}} \text{ mJy}, \quad (\text{B8})$$

$$F_\nu \stackrel{(8a)}{=} 10^{\frac{2p^2-7.7p+0.8}{4-p}} D_{28}^{-2} \left[E_{53}^{\frac{1}{4}(12-p^2)} n_{*,0}^{-\frac{1}{2}(p-2)} \varepsilon_{e,-1}^{(p-1)(3-p)} \varepsilon_{B,-4}^{\frac{1}{4}(-p^2+2p+4)} \right]^{\frac{1}{4-p}} \nu_{17.5}^{-\frac{p}{2}} T_{d,-1}^{-\frac{3p}{4} + \frac{1}{4-p}} \text{ mJy} \quad (2 < p < 3). \quad (\text{B9})$$

The case given in equation (B9) and labeled (8a) corresponds to the same frequency ordering as for case (8), but the cooling break ν_c evolution (eq. [45]) is determined by the IC losses, i.e. $T_r < T < T_y$ and $Y_a > 1$.

WIND EXTERNAL MEDIUM ($S = 2$)

Following the same exercise as above and using the relevant equations, the following results can be obtained for the wind model:

$$F_\nu \stackrel{(1)}{=} 0.03 D_{28}^{-2} (Y_r + 1)^{-1} E_{53} A_*^{-2} \varepsilon_{e,-1}^{-1} \varepsilon_{B,-2}^{-1} \nu_{9.7}^2 T_{d,-1}^2 \text{ mJy}, \quad (\text{C1})$$

$$F_\nu \stackrel{(2)}{=} 70 D_{28}^{-2} (Y_r + 1)^{2/3} E_{53}^{1/3} A_*^{5/3} \varepsilon_{B,-2} \nu_{12}^{1/3} T_{d,-1}^{-2/3} \text{ mJy}, \quad (\text{C2})$$

$$F_\nu \stackrel{(5)}{=} 0.07 D_{28}^{-2} E_{53} A_*^{-1} \varepsilon_{e,-1} \nu_{9.7}^2 T_{d,-1} \text{ mJy}, \quad (\text{C3})$$

$$F_\nu \stackrel{(6)}{=} 9 D_{28}^{-2} E_{53}^{1/3} A_* \varepsilon_{e,-1}^{-2/3} \varepsilon_{B,-3}^{1/3} \nu_{12}^{1/3} T_d^0 \text{ mJy}, \quad (\text{C4})$$

$$F_\nu \stackrel{(7)}{=} 10^{2.3-1.2p} D_{28}^{-2} E_{53}^{\frac{p+1}{4}} A_* \varepsilon_{e,-1}^{p-1} \varepsilon_{B,-4}^{\frac{p+1}{4}} \nu_{14.6}^{-\frac{p-1}{2}} T_d^{-\frac{3p-1}{4}} \text{ mJy}, \quad (\text{C5})$$

$$F_\nu \stackrel{(8a)}{=} 10^{\frac{1.9p^2-8.6p+5.4}{4-p}} D_{28}^{-2} E_{53}^{\frac{p+2}{4}} \left[A_*^{-(p-2)} \varepsilon_{e,-1}^{(p-1)(3-p)} \varepsilon_{B,-4}^{\frac{1}{4}(-p^2+2p+4)} \right]^{\frac{1}{4-p}} \nu_{17.5}^{-\frac{p}{2}} T_{d,-1}^{-\frac{3p}{4} + \frac{p}{2(4-p)}} \text{ mJy} \quad (2 < p < 3). \quad (\text{C6})$$

For the remainder of the cases it can be shown that the fluxes for the wind model differ from those for obtained in the $s = 0$ model only by a constant factor:

$$\frac{F_\nu(s=2)}{F_\nu(s=0)} \stackrel{(3)}{=} 0.60 \frac{Y_r(s=0)}{Y_r(s=2)}, \quad (\text{C7})$$

$$\frac{F_\nu(s=2)}{F_\nu(s=0)} \stackrel{(4)}{=} 1.24 \left(\frac{17}{72} \right)^{p/4} \frac{Y_r(s=0)}{Y_r(s=2)}, \quad (\text{C8})$$

$$\frac{F_\nu(s=2)}{F_\nu(s=0)} \stackrel{(8)}{=} 1.35 \left(\frac{17}{72} \right)^{p/4}. \quad (\text{C9})$$

This means that observations made at frequencies above the cooling break are unable to distinguish between the two models for the external medium, with the exception of the case where the electron cooling is dominated by IC losses (case 8a).

The reference frequency in the equations above was chosen $\nu = 4 \times 10^{14}$ Hz whenever this optical frequency falls in one of the cases labeled in equations (65)–(66), for the model parameters given in Figures 1 and 2. The observer time was scaled to a value at which each case is more likely to occur.

The above light-curves must be corrected to account for cosmological effects. This is achieved by replacing T with $T/(1+z)$ and ν with $(1+z)\nu$, where z is the burst redshift.

TABLE 1.

VALUES OF THE FACTOR K GIVEN IN EQUATION (A3), REPRESENTING THE CORRECTION THAT SHOULD BE APPLIED TO THE ANALYTICAL LIGHT-CURVES TO ACCOUNT FOR THE EFFECTS DUE TO THE REMNANT GEOMETRICAL CURVATURE.

s	(1)	(2)	(3)	(4)*	(5)	(6)	(7)*	(8)*
0	0.50	0.55	0.59	1.37	1.00	0.42	1.34	1.02
2	0.11	1.76	0.74	1.19	0.12	0.90	2.25	0.82

* in this case K depends on p . The values given here are for $p = 2.5$.

REFERENCES

- Blandford, R. D. & McKee, C. F. 1976, *Phys. Fluids*, 19, 1130
 Bloom, J. et al. 1999, *Nature*, 401, 453
 Chevalier, R.A. & Li, Z.-Y. 1999, *ApJ*, 520, L29
 Chevalier, R.A. & Li, Z.-Y. 2000, *ApJ*, in press (astro-ph/9908272)
 Dai, Z. & Lu, T. 2000, *ApJ*, in press (astro-ph/9906109)
 Fenimore, E.E. & Ramirez-Ruiz, E. 2000, *ApJ*, submitted (astro-ph/9909299)
 Frail, D. et al. 2000, *ApJ*, submitted (astro-ph/9910060)
 Frail, D., Waxman, E., & Kulkarni, S. 2000, *ApJ*, submitted (astro-ph/9910319)
 Galama, T. et al. 2000, *ApJ*, submitted (astro-ph/9907264)
 Goodman, J. 1997, *New Astronomy*, 2, 449
 Granot, J., Piran, T., & Sari, R. 2000, 534, L163
 Groot, P. et al. 1998, *ApJ*, 502, L123
 Halpern, J., Kemp, J., Piran, T., & Bershad, M. 1999, *ApJ*, 517, L105
 Harrison, F. et al. 1999, *ApJ*, 523, L121
 Kulkarni, S. et al. 1999a, *Nature*, 398, 389
 Kulkarni, S. et al. 1999b, *ApJ*, 522, L97
 Kumar, P. & Panaitescu, A. 2000, *ApJL*, submitted (astro-ph/0003264)
 Mészáros, P. & Rees, M. J. 1997a, *ApJ*, 476, 232
 Mészáros, P. & Rees, M. J. 1997b, *ApJ*, 482, L29
 Paczyński, B. & Xu, G. 1994, *ApJ*, 427, 708
 Paczyński, B. 1998, *ApJ*, 494, L45
 Panaitescu, A. & Mészáros, P. 1998, *ApJ*, 493, L31
 Piran, T. 1999, *Physics Reports*, 314, 575
 Rees, M.J. & Mészáros, P. 1994, *ApJ*, 430, L93
 Reichart, D. 1999, *ApJ*, 521, L111
 Rhoads, J. E. 1999, *ApJ*, 525, 737
 Rybicki, G.B. & Lightman, A.P. 1979, *Radiative Processes in Astrophysics* (New York : Wiley-Interscience)
 Sari, R., Piran, T., & Narayan, R. 1998, *ApJ*, 497, L17
 Sari, R. & Piran, T. 1999, *ApJ*, 520, 641
 Stanek, K., Garnavich, P., Kaluzny, J., Pych, W., & Thompson, I. 1999, *ApJ*, 522, L39
 Waxman, E. 1997a, *ApJ*, 485, L5
 Waxman, E. 1997b, *ApJ*, 489, L33
 Wei, D. & Lu, T. 1998, *ApJ*, 505, 252
 Wijers, R. & Galama, T. 1999, *ApJ*, 523, 177
 Woosley, S. 1993, *ApJ*, 405, 273

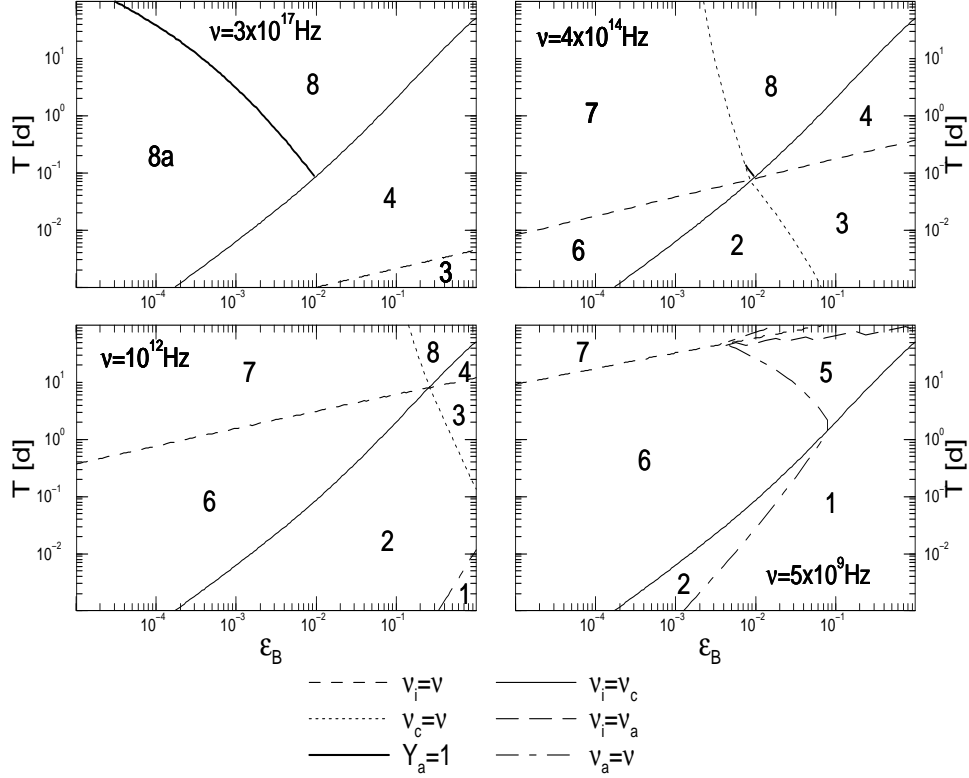


FIG. 1.— The afterglow brightness at a given frequency (indicated in each panel) is dependent on the relationship between this frequency and those of the injection (ν_i), cooling (ν_c), and absorption (ν_a) breaks. Different combinations of these four frequencies are indicated in the *time* – ϵ_B plane for the homogeneous external medium model ($s = 0$), according to the labeling given in equations (65) – (66). The label 8a indicates the case when $\nu_i < \nu_c < \nu$ and $Y_a > 1$, i.e. the cooling break ν_c evolution is determined by the IC losses. Other model parameters are $E = 10^{53}$ erg (in 4π sr), $n_* = 1 \text{ cm}^{-3}$, $\epsilon_e = 0.1$, and $p = 2.5$. The upper two panels also indicate the time when the Compton parameter Y_a for adiabatic electrons becomes unity.

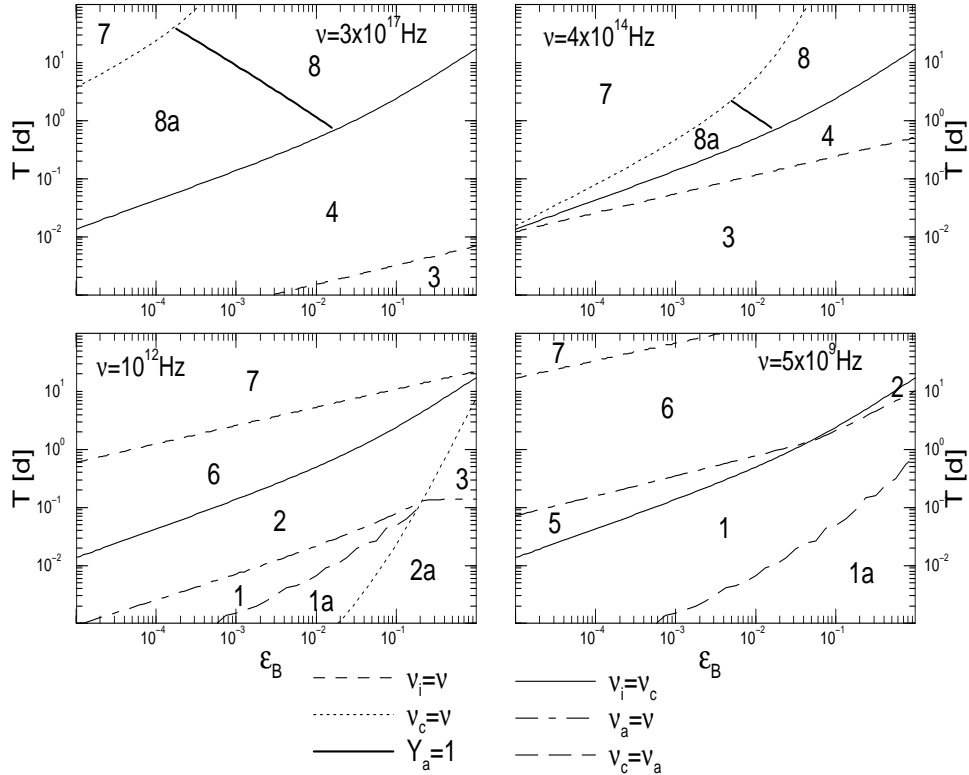


FIG. 2.— Same diagrams as for Figure 1, but for a wind model ($s = 2$) with $A_* = 1$.

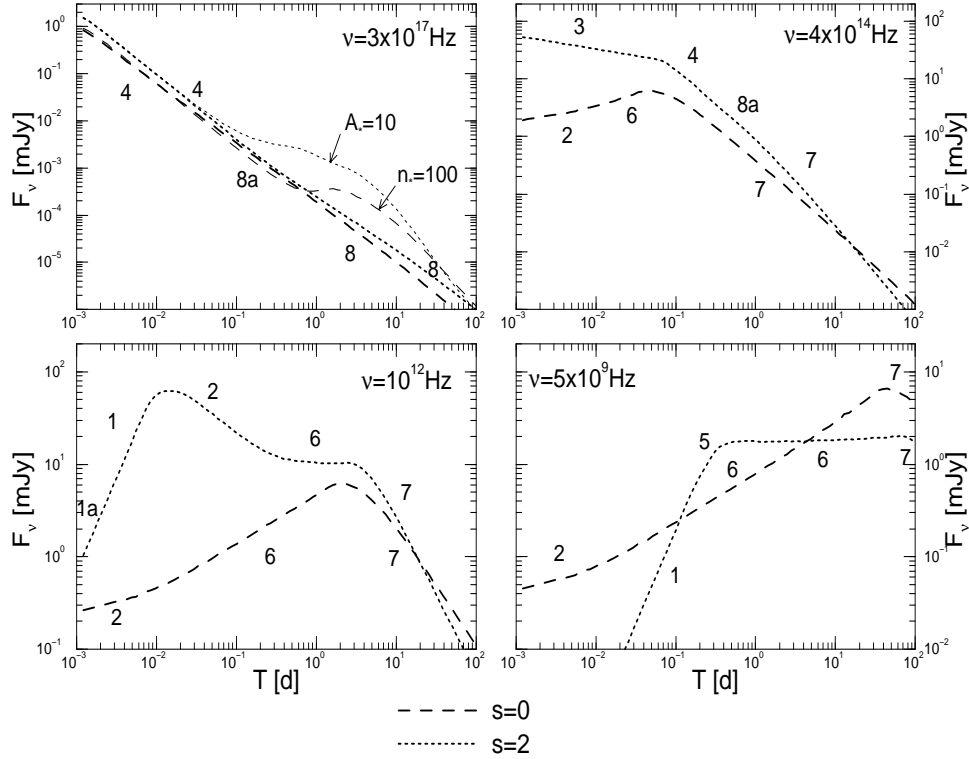


FIG. 3.— Numerical light-curves for $D = 10^{28}$ cm, $E = 10^{53}$ erg (in 4π sr), $\varepsilon_e = 0.1$, $\varepsilon_B = 10^{-3}$, $p = 2.5$, for a homogeneous external medium (dashed lines) with $n_* = 1 \text{ cm}^{-3}$ and a pre-ejected wind (dotted lines) with $A_* = 1$, at various observing frequencies (given in each panel). The numbers indicate the cases identified in equations (65) - (66). The afterglow emission is calculated using equations that are valid in any relativistic regime. The effect of the remnant geometrical curvature on the photon arrival time and relativistic boosting are taken into account.

Note that the largest differences between the two models are shown by the low frequency light-curves at observer times below ~ 1 day.

Also shown in the upper left panel are two soft X-ray light-curves for denser external media: $n_* = 10^2 \text{ cm}^{-3}$ for $s = 0$ (thin dashed curve) and $A_* = 10$ for $s = 2$ (thin dotted line), in which cases the afterglow emission at $T \gtrsim 10^{-1}$ day is dominated by IC scatterings, and exhibits a substantial flattening. Such a feature is chromatic and cannot be seen at lower observing frequencies. The flattening of the X-ray emission in the case of denser media is present for other plausible sets of model parameters, as long as they lead to fluxes (at the time when the flattening occurs) that are detectable with current instruments.

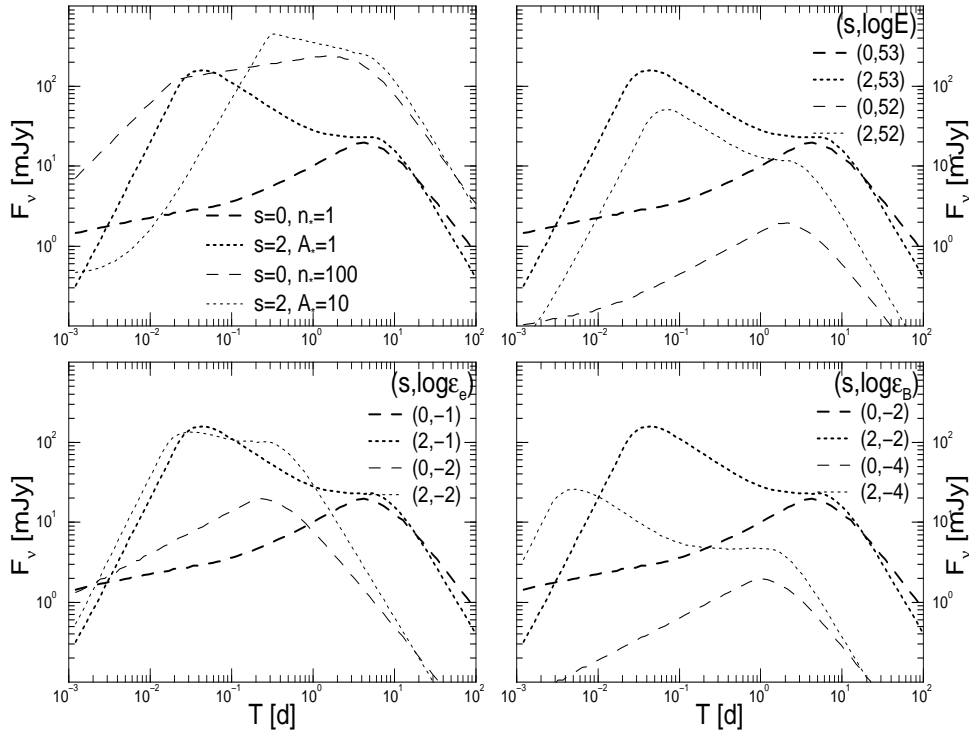


FIG. 4.— Comparison between the afterglow light-curves at observing frequency $\nu = 10^{12}$ Hz for homogeneous external media (dashed lines) and pre-ejected winds (dotted lines), and for various model parameters, as given in each panel. Unless specified in the legend, the model parameters are $E = 10^{53}$ erg (in 4π sr), $n_* = 1 \text{ cm}^{-3}$, $A_* = 1$, $\varepsilon_e = 0.1$, $\varepsilon_B = 10^{-2}$, and $p = 2.5$.